Abrupt Intense Radiation from Divertor Plates of the Large Helical Device

K. Narihara, I. Yamada, T. Minami and H. Hayashi

National Institute for Fusion Science, Toki 509-5292, Japan

This paper examines the phenomenon of abrupt intense radiation (AIR) from a graphite divortor plate measured by the DC-coupled Thomson scattering detectors on LHD. A time-integrated spectrum of this AIR resembles to a black body (BB) radiation mixed with plasma light line-radiation. We estimate the BB-radiation temperature from the ratios among signals from a five-color-channel polychromator. The BB-radiation temperature T_B, thus obtained, abruptly rises up to ~2000K and after some duration rapidly decays usually after a small drop in NBI power. Time evolution of BB radiation intensity calculated with this T_B well reproduces the observed signals. The experimental data are compared with 1D thermal transport simulations in graphite plate taking account of the nonlinear diffusivity. With the conventional thermal conduction model, including non-linear thermal diffusivity, the observed rapid T_B rise cannot be reproduced. Correlations between the size of AIR and various plasma/operational parameters are presented.

Keywords: Thomson scattering diagnostic, LHD, divertor plate

1. Introduction

Background radiation has degrading effects on Thomson scattering (TS) diagnostics [1]: it drops S/N ratio and sometimes introduces large systematic errors into the obtained data. In an extreme case the electron temperature (*Te*) and density (*ne*) profiles collapse as shown later. Even if the size of collapse is small, without quantitative data on the radiation intensity, the confidence on the obtained *Te* and *ne* profiles is low. In order to solve this problem to some extent, we installed 1040-channel scanning ADC so that the DC levels of the avalanche photo-diodes used for detecting the scattered light can be monitored. With this background light monitoring, we found that an abrupt intense radiation (AIR) often appears around divortor plates and invalidates TS data greatly. Intending to suppress or reduce the AIR, we examine this phenomenon.

2. Description of AIR

Figure 1(A) shows a *Te* and *ne* profiles with large collapse. The collapsed region coincides roughly with the scattering region that has a divortor plate in background scope of the light collection optics. The DC-coupled outputs (*DC_APD*) from light detectors 'seeing' this region exceed greatly 0.6V, which is upper limit for linearity for pulse response, thus invalidating the obtained data. (For DC response, linearity is preserved up to ~4 V.) It should be noted that the focal points of the light collection optics are on the laser beam, and hence the spatial distribution of *DC_APD*, Fig 1. (B), is not a real distribution but a convolution of it. Figure 2 shows

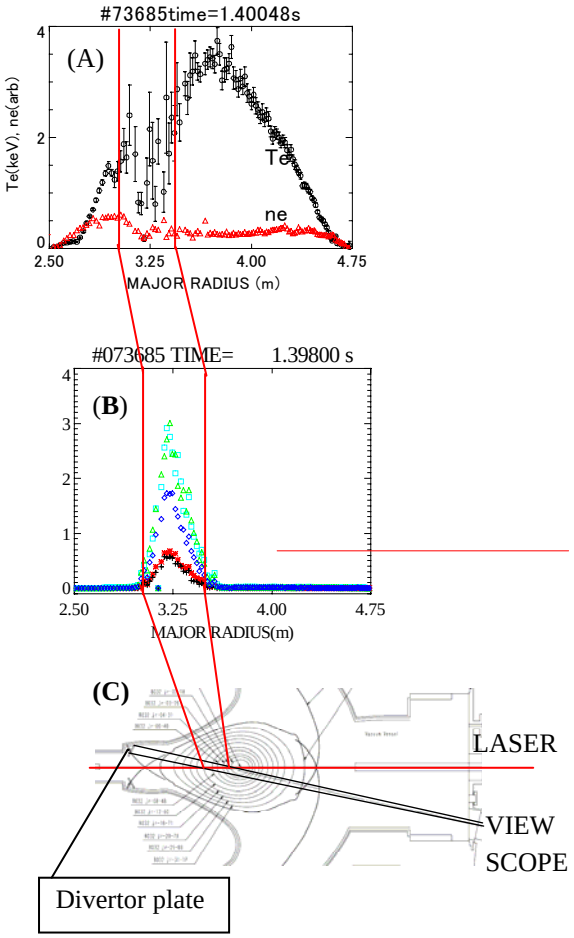

Fig. 1. (A) Collapsed Te and ne profiles. (B) Distribution of DC-outputs of APDs. (C) Thomson scattering configuration [2].

author's e-mail:narihara@nifs.ac.jp

the time evolutions of the 5-color-channel *DC_APD* signals from the polychromator#32 together with relevant plasma parameters. We can see that *DC_APD* starts to grow after additional NBI start its operation. It is hard to find a signal that well correlates with the startup of AIR.

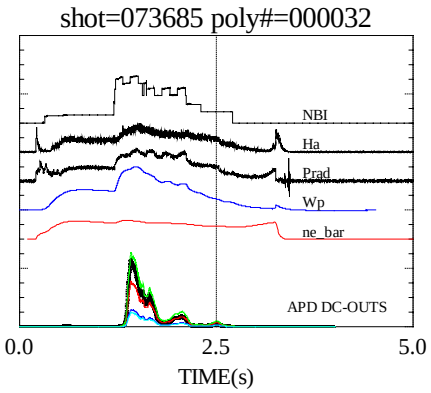

Fig. 2. Time evolutions of DC_APD together with the cord-averaged plasma density ne_bar, the diamagnetic energy Wp, the bolometer signal Prad, H-alpha, and total NBI power.

There seems to be a tendency, however, that an AIR sometimes appears at the time when the diamagnetic signal *Wp* approaches its peak. From the energy-flow equation: P_{heat}= dW/dt + P_{out} + P_{rad}, where P_{heat} is heating power, P_{out} is the wall loading power carried by particles and P_{rad} is radiation loss from plasma, the above statement leads us to an assumption that the AIR appears when P_{out} becomes large. This assumption is further supported by facts that there is a lower threshold in NBI power for AIR to occur and that the higher P_{rad} often reduces the size of AIR. Figure 3 (A) shows a time-integrated spectrum of the AIR appeared on the same shot as in Fig. 2 measured by a fiber-multi-channel spectrometer. The 3073K black body radiation spectrum from a standard lamp measured by the same spectrometer is shown in Fig. 3(B) for a reference. The spectrum of the AIR resembles well black body radiation.

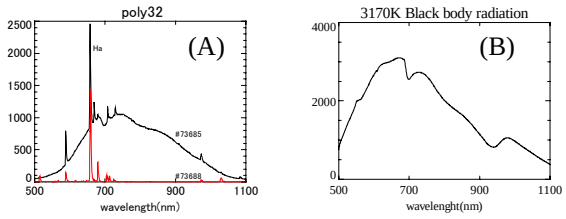

Fig. 3. (A) Time integrated multi-channel-spectrum of the light from the fiber connected to poly32 with/without AIR. (B) A 3170K BB radiation spectrum measured by the same spectrometer.

Assuming the black body radiation, we can estimate effective temperature of the AIR using the currently used polychromators, the spectrum of which is shown in Fig.4 (A) together with the BB radiation of various temperatures. The ratios F5/F1, F4/F1, F3/F1, F2/F1 as a function of T_B are shown in Fig. 4(B). The T_B that best fits to the observed signals as a function of time is shown in Fig. 5(A). The upper- and –lower limits of the error bars are given by the roots of the equation H(T_B)=2*min(H(T_B)), where H is the residual square sum of the fitting. In the calculation, we set T_B =0 for signal < 10mV, to avoid large irregularities in T_B for small signals. Using this T_B-evolution, we can calculate the time evolution of signals as shown in Fig. 5(B), which surprisingly well reproduces the observed signals, Fig. 5(C) after signals reach their peaks. Here we assume that the BB emitting area is held constant. Although the BB assumption seems to approximately explain the observation, there is a difficulty in the startup phase: The T_B grows in a few ms, which is too rapidly to be realistic.

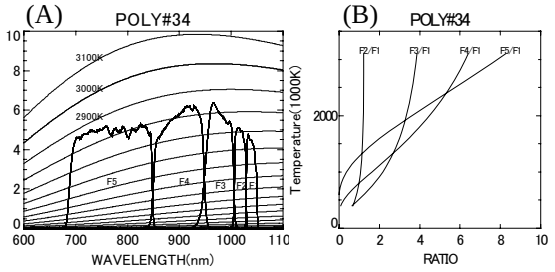

Fig. 4. (A) Responsivities of 5-color- polychromator #34 and BB radiation spectra of various temperatures. (B) Signal ratios among the five outputs vs. temperature.

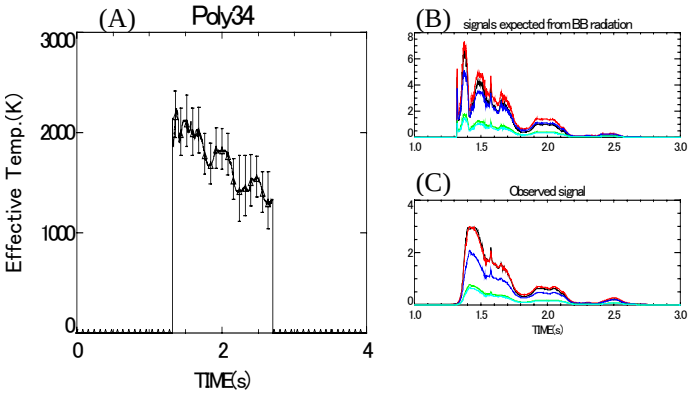

Fig. 5. (A) Deduced temperature evolution. (B). Calculated signal sizes from BB radiation of temperature shown left. (C): The observed signal size. Both waveforms are similar in shape.

3. 1D simulation

In order to examine the above fast rise of T_B, we consider 1D heat conduction model described below. One side of a graphite (x=0) is exposed to a heat flux q and emits BB-radiation σTs^4, where Ts is the surface temperature, and other end surface (x=15mm) is kept at a constant temperature T(15)=300K. We assume the heat is deposited in the surface layer of thickness τ. The heat diffusivity decreases rapidly as temperature rises as shown in Fig.6(B) [3], the non-linearity of which is expected to accelerate the temperature rise. An example of the numerical solution of the heat conduction equation

$$\frac{\partial T}{\partial t} = \alpha(T)\frac{\partial^2 T}{\partial x^2},$$

with boundary conditions

$$c\rho\tau\frac{\partial T_s}{\partial t} = q - \sigma T_s{}^4 + k\frac{\partial T_s}{\partial x}$$

and

$$T(15,t) = 300,$$

where c is heat capacity, ρ density, τ the thickness of heat deposition, σ Stefan-Boltzmann coefficient, k the heat conductivity, is shown in Fig. 6(A). We can see that as *q* increases the rise time becomes faster and the attainable temperature is higher. Within the above conventional model of heat conduction, we cannot reproduce the observed behavior of *Ts*. An exotic model such as bubbles or a crack formation beneath the heated surface, which switches off the heat conduction, may reproduce the observation. With this fast rise problem, we now hesitate to conclude the AIR is BB radiation. Further diagnostics such as IR camera will help us draw a conclusion.

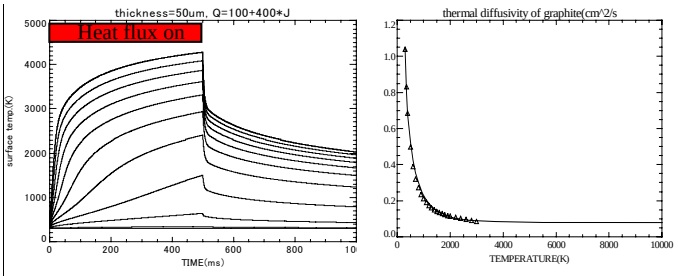

Fig. 6. Right: thermal heat diffusivity of graphite, which is highly non-linear function of temperature. Left: Examples of surface temperature evolutions for various heat flux. Heat deposition layer thickness is 50 μm. The top curve is Ts for q=3.7 kW/cm^2: From the top, q decreases by 400W/cm^2 from curve to curve.

4. Statistics

In order to get clues to the question what the AIR really is, we took statistics of the size of the AIR as a function of various operation/plasma parameters. Figure 7 shows the *DC_APD* distribution as a function of the major radius. The larger *DC_APD* appear in the range 3.6m≦ Rax ≦3.75m. Although the shot numbers on bins are largely different, they are large enough, except extremely inwards shifted cases, to show the general tendency. This tendency may be explained by fact that the particle/heat flux to inner-divertors is smaller for the outwards shifted configurations. Figure 8 shows *DC_APD* as a function of magnetic field intensity on the axis. There is a clear tendency that at higher magnetic fields, AIR is larger. This suggests that a stronger magnetic field may focus plasma flow more effectively to the divertor plate. Figure 9, bolometer signal vs. the size of AIR, indicates they anti-correlate. This seems to support our assumption that AIR is caused by heat flux to the divertor plate:

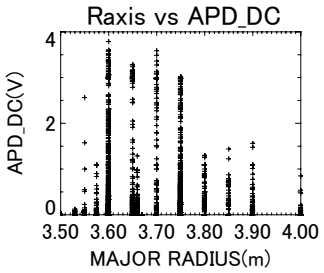

Fig. 7. Major radius vs. AIR size.

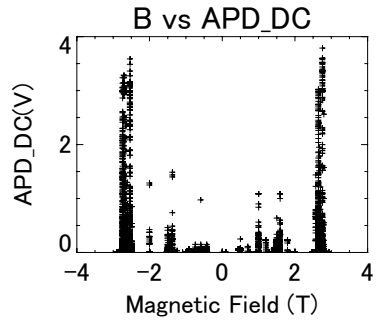

Fig. 8. Magnetic field intensity on the axis vs. AIR size.

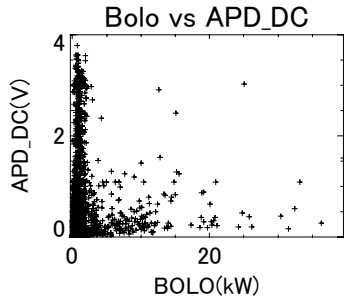

Fig. 9. Bolometer signal vs. AIR size.

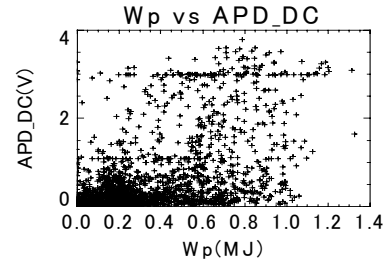

Fig. 10. Wp vs. AIR size.

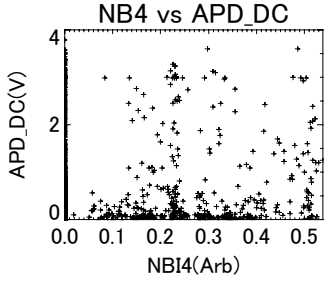

Fig. 11. NB4 injection power vs. AIR size.

higher radiation power lessens the wall-loading power, provided that the total loss power is held constant. Figure 10, *Wp* vs. AIR size relation, shows no correlation between them.

NB4 is injected in the radial direction, whereas the other NB, NB1, NB2 and NB3, are injected in tangential directions. It is expected that appreciably amount of the radially injected NB is promptly lost and hit divertor plate. In this respect, it is curious to investigate the correlation between NB4 power and AIR size. Figure 11 gives this. No correlation can be seen.

If the AIR is plasma light generated around the graphite divertor plate, it will accompany appreciable signal on the CIII-line-monitor installed on 1-O-port. Figure12, CIII vs. AIR size relation, however, reveals no positive correlation.

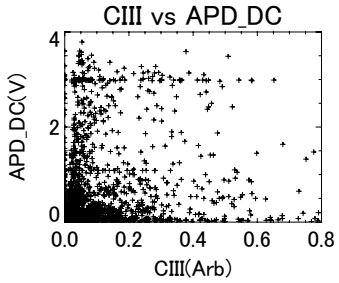

Fig. 12. CIII radiation vs. AIR size.

Figure 13 shows the distribution of *DC_APD* as a function of line averaged plasma density. There seems a high occurrence region in the lower density, but its significance is not yet clear.

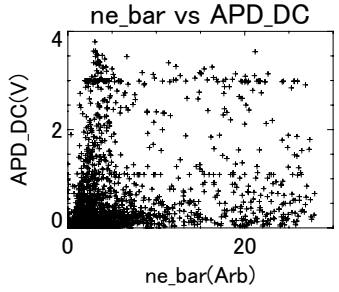

Fig. 13. ne_bar vs. AIR size.

5. Discussions and summary

The AIR poses a serious problem to the Thomson scattering diagnostic, but it seems that it has no appreciable adverse effect on the core plasma confinement. If the AIR is only black body radiation from the heated graphite plate, it is quite natural. On the other hand, if the AIR is radiation from plasma created on the surface of the divortor plate, there may be carbon impurity influx to the core plasma. But, up to now, no such indication has been observed. Even if the AIR is plasma radiation, the existence of the so-called stochastic region will shield the impurity influx efficiently.

We have not yet obtained a definite conclusion what the AIR really is. Probably, it is black body radiation from the heated divertor plate. But its very rapid rise makes us to hesitate to take this simple view. We are planning to replace the divertor plate with a new one with much higher heat conductance.

References

[1] K.Narihara, et al., *in ITC-16 proceedings, (2006).*

[2] K.Narihara, et al., Rev. Sci. Instrum. 72, 1122(2001).

[3] Thermo-physical properties of matter, Volume 10. Thermal Diffusivity, IFI/Plenum, New York-Washington 1970.